



Since January 2020 Elsevier has created a COVID-19 resource centre with free information in English and Mandarin on the novel coronavirus COVID-19. The COVID-19 resource centre is hosted on Elsevier Connect, the company's public news and information website.

Elsevier hereby grants permission to make all its COVID-19-related research that is available on the COVID-19 resource centre - including this research content - immediately available in PubMed Central and other publicly funded repositories, such as the WHO COVID database with rights for unrestricted research re-use and analyses in any form or by any means with acknowledgement of the original source. These permissions are granted for free by Elsevier for as long as the COVID-19 resource centre remains active.



Proposal of novel natural inhibitors of severe acute respiratory syndrome coronavirus 2 main protease: Molecular docking and *ab initio* fragment molecular orbital calculations

Divya Shaji^a, Shohei Yamamoto^b, Ryosuke Saito^b, Ryo Suzuki^b, Shunya Nakamura^b, Noriyuki Kurita^{b,*}

^a Independent Researcher, Kerala 680642, India

^b Department of Computer Science and Engineering, Toyohashi University of Technology, Tempaku-cho, Toyohashi, Aichi 441-8580, Japan

ARTICLE INFO

Keywords:

COVID-19
SARS-CoV-2
Main protease
Moringa oleifera
Natural product
In silico drug design
Molecular simulation
Molecular docking
Fragment molecular orbital

ABSTRACT

This paper proposes natural drug candidate compounds for the treatment of coronavirus disease 2019 (COVID-19). We investigated the binding properties between the compounds in the *Moringa oleifera* plant and the main protease (Mpro) of severe acute respiratory syndrome coronavirus 2 using molecular docking and *ab initio* fragment molecular orbital calculations. Among the 12 compounds, niaziminin was found to bind the strongest to Mpro. We furthermore proposed novel compounds based on niaziminin and investigated their binding properties to Mpro. The results reveal that the introduction of a hydroxyl group into niaziminin enhances its binding affinity to Mpro. These niaziminin derivatives can be promising candidate drugs for the treatment of COVID-19.

1. Introduction

The outbreak of the novel coronavirus disease 2019 (COVID-19) caused by severe acute respiratory syndrome coronavirus 2 (SARS-CoV-2), has raised serious global health concerns. On March 11, 2020, the World Health Organization officially declared the SARS-CoV-2 outbreak a pandemic [1]. Coronaviruses are large RNA viruses belonging to the Coronaviridae family, which is further categorized into four genera, *i.e.*, alpha, beta, gamma, and delta coronaviruses. Typically, the former two infect mammals, whereas the latter two infect birds [2,3]. SARS-CoV-2 is a beta coronavirus. To date, no specific antiviral drugs are available for the treatment of COVID-19 [4], although several clinical trials are currently underway to identify effective drugs. In the development of these drugs, it is essential to identify and evaluate novel drug lead compounds for treating COVID-19. In the present study, using molecular docking and *ab initio* molecular orbital calculations, we attempt to establish the specific compounds of the *Moringa oleifera* (*M. oleifera*) plant that can bind strongly to the SARS-CoV-2 main protease (Mpro) and inhibit its activity.

The Mpro plays a major role in mediating the replication and

transcription of SARS-CoV-2. The mutagenesis rate is low in the Mpro, and it cleaves the pp1a and pp1b polyproteins, which release functional proteins, including RNA polymerase, exoribonuclease, and endoribonuclease [5,6]. Moreover, Mpro inhibitors are considered less cytotoxic because of the low similarity between Mpro and human proteases [7–9]. Therefore, the Mpro is a promising target for drugs with which to treat coronaviruses, and the inhibition of Mpro activity is vital to blocking coronavirus replication [5,9,10].

To date, several studies have focused on the inhibition of Mpro activity [5–7]. Pendyala et al. [11] conducted molecular docking studies to identify potential inhibitors for the Mpro and the RNA-dependent RNA polymerase in bioactive food compounds. Their results showed that phycocyanobilin, riboflavin, cyanidin, daidzein, and genistein were more potent as Mpro inhibitors than antiviral drugs (remdesivir, nelfinavir, and lopinavir). Similarly, on the base of molecular docking simulations, Das et al. proposed a natural compound, rutin, which had the highest inhibitor efficiency among the 33 compounds they studied [12]. Theaflavin digallate, which is an antioxidant natural phenol and a theaflavin derivative found in black tea, was shown to bind strongly to the target Mpro [13]. Furthermore, Gurung et al. reported that bonducellpin

* Corresponding author.

E-mail address: kurita@cs.tut.ac.jp (N. Kurita).

<https://doi.org/10.1016/j.bpc.2021.106608>

Received 11 March 2021; Received in revised form 19 April 2021; Accepted 26 April 2021

Available online 29 April 2021

0301-4622/© 2021 Elsevier B.V. All rights reserved.

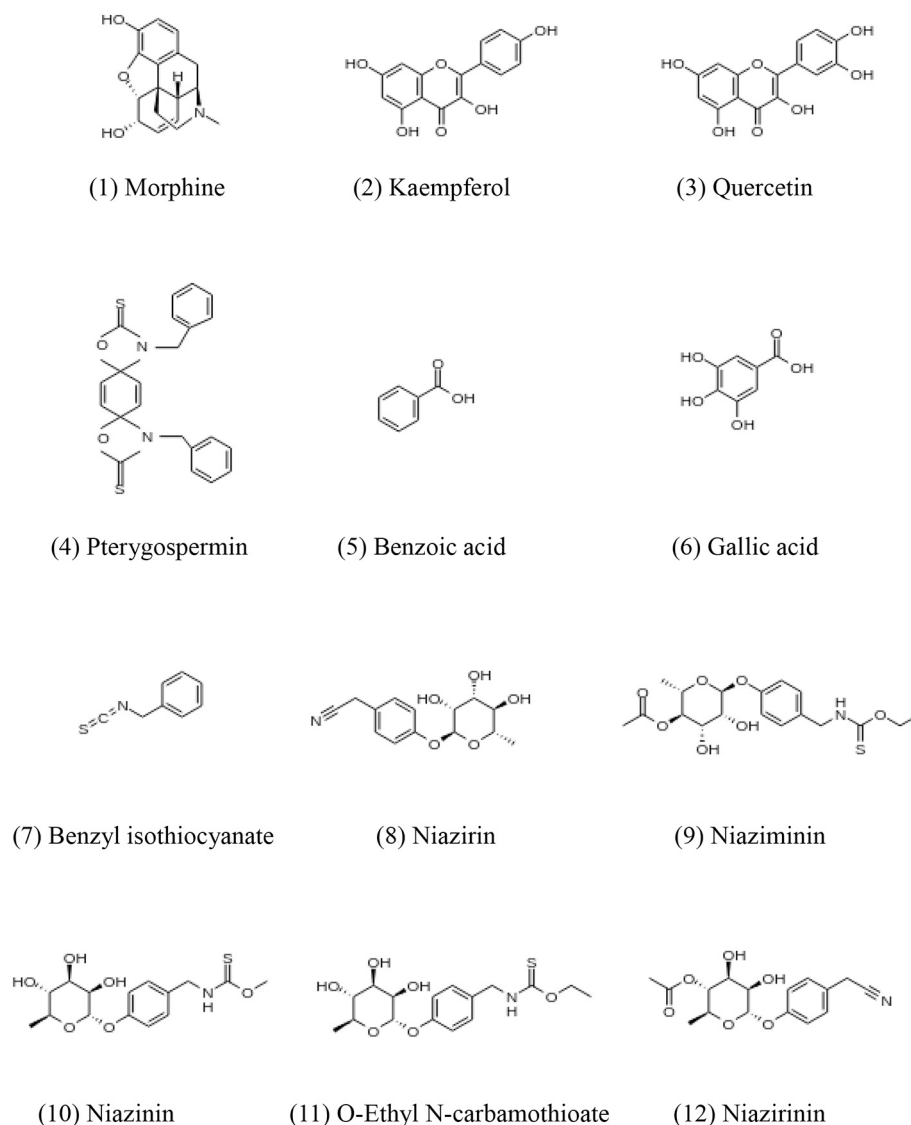


Fig. 1. The chemical structures of the 12 compounds found in *Moringa oleifera*.

D, a furanoditerpenoid lactone isolated from *Caesalpinia minax*, exhibited a high binding affinity toward the Mpro [14].

Natural compounds play an important role in the treatment of a wide range of diseases [15]. For example, *M. oleifera* is a plant belongs to the *Moringaceae* family, originating in India. It is cultivated commercially in Africa, Mexico, the United States (including Hawaii), and across Asia. Its antifungal, antioxidant, antibacterial, anti-inflammatory, diuretic, and hepato-protective properties has been studied [16]. Several studies have reported the antiviral activity of *M. oleifera*, and the plant has been used in many traditional medicines. It has proved to be effective at fighting several viruses, such as the human immunodeficiency virus (HIV), the herpes simplex virus, hepatitis B virus, Epstein–Barr virus (EBV), foot-and-mouth disease virus, and Newcastle disease virus. Moreover, it has been used for the treatment of HIV-related diseases in African countries [17].

In a previous study [16], the antiviral properties of *M. oleifera* in Huh7 cells were evaluated. *M. oleifera* is known to contain several bioactive compounds that include phenolic acids, flavonoids, alkaloids, vitamins, tannins, saponins, and isothiocyanates. The different parts of *M. oleifera* such as root, leaf, seed, flower etc. exhibit various biological activities. Furthermore, *M. oleifera* was found to improve hepatic and renal functions, as well as the regulation of thyroid hormone status

[18–21].

The present study aims to discover natural inhibitors of the SARS-CoV-2 Mpro. To identify novel drug lead compounds for the inhibitor, we first investigated the specific interactions between the Mpro and the 12 natural compounds found in *M. oleifera* at an electronic level, using molecular docking, classical molecular mechanics (MM), and *ab initio* fragment molecular orbital (FMO) simulations. Among the 12 compounds, we determined which could bind strongly to the Mpro and be potential lead compounds for Mpro inhibitors. Additionally, we proposed novel compounds based on the most promising lead compound and investigated their binding properties to the Mpro to derive novel natural Mpro inhibitors. These simulated results will be useful for designing novel natural drugs to target the Mpro of SARS-CoV-2.

2. Details of molecular simulations

2.1. Construction and optimization of the Mpro + compound complexes

Data on the compounds contained in the various parts of *M. oleifera* were collected from the literature [18–21]. The initial dataset included 33 compounds. These were filtered using “Lipinski’s rule of five” [22], which is important for the screening of drugs with pharmacological

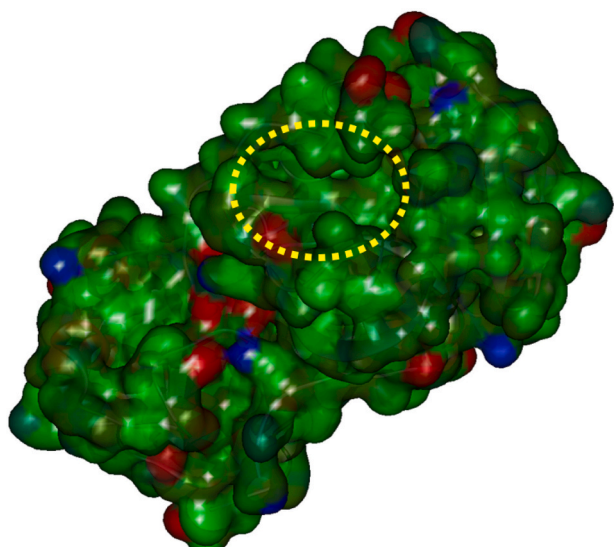


Fig. 2. Structure of Mpro and its ligand-binding pocket marked by a yellow ellipse. Charge distribution on Mpro is shown in red (negative), blue (positive), and green (neutral), respectively. (For interpretation of the references to colour in this figure legend, the reader is referred to the web version of this article.)

activity. To predict the chemical properties of the compounds, we used the SwissADME web tool [23]. As listed in Table S1 of the Supplementary Information (SI), only 12 of the 33 compounds satisfied Lipinski's rule. We used these 12 compounds [24] shown in Fig. 1 as lead candidates for the Mpro inhibitor. Their three-dimensional (3D) structures were obtained from a structure data file format in the PubChem database [25].

The structures of the 12 compounds were fully optimized in a vacuum using the B3LYP/6-31G(d,p) method of the *ab initio* molecular orbital calculation program Gaussian 09 (G09) [26]. The charge distributions of the optimized structures were evaluated using restrained electrostatic potential (RESP) analysis [27] of G09 using the HF/6-31G(d) method, and the RESP charges were employed as the charge parameters in the MM force fields of the compounds. These RESP charges were essential to the docking simulations, along with the MM optimizations of the Mpro + compound complexes, to precisely describe the electrostatic interactions between the Mpro and each of the compounds.

The 3D structure of the Mpro was downloaded from the Protein Data Bank (PDB ID: 6LU7) [28]. This Mpro has seven histidine (His) residues, each of which can have three types of protonation states (Hid, Hie, and Hip⁺), depending on the pKa values around them. When His residues have a pKa value greater than 6, they prefer a protonated Hip⁺ state, whereas other His residues can possess Hid or Hie states, depending on the structure around them. To predict the pKa values for the His residues, we used the PROPKA3.1 software [29,30]. Of the seven His residues, only His64 was assigned as Hip⁺. His41, His80, His163, and His172 were assigned to the Hid state, whereas His164 and His246 were assigned to the Hie state, considering the structures around these His residues. For the remaining ionizable amino acid residues in the Mpro, an ionized state was adopted.

Fig. 2 shows the ligand binding pocket of Mpro [28]. To find the binding site of the compound in the pocket, we conducted molecular docking studies using AutoDock4.2.6 [31]. In the docking simulations, the size of the grid box was set to 19.5 × 19.5 × 19.5 Å³, which is almost 1.5 times the size of the compound, and the center of the grid box was set to the center of the ligand in the PDB structure [28] of the Mpro + ligand complex. The number of created candidate poses was 256, and the threshold distance for clustering these poses was set as 2 Å. From the various clusters generated by AutoDock [31], we selected the three with the largest number of poses, and the representative structures of these

clusters were used in the subsequent MM and FMO calculations.

To obtain stable structures for the Mpro + compound complexes, the representative structures of the clusters obtained from the docking simulations were fully optimized in water using the classical MM method. In the MM optimizations, approximately 1800 water molecules existing within 8 Å of the complex surface were explicitly considered. The MM and molecular dynamics simulation program AMBER 12 [32] was used. The AMBER FF99-SBLLIN force field [33], TIP3P model [34], and general AMBER force field [35] were assigned to the Mpro, water molecules, and compounds, respectively. The criterion for the convergence of structure optimization was set as 0.0001 kcal/mol/Å.

Table 1

Lowest binding energy (BE: kcal/mol), number of poses, and Mpro residues involved in H-bonds with each compound for the selected clusters obtained by AutoDock4.2.6 program [31].

Compound	Cluster	BE	Poses	Residues involved in H-bonds	IFIE
1	2	-5.18	141	Glu166	-41.4
	3	-5.13	77	Gln189	-67.0
	5	-4.82	33	Thr24, Thr26	-66.3
2	1	-4.65	52	Thr24, Thr26, Asn142, His163	-55.0
	2	-4.58	131	Thr26, Leu141, Gly143, Ser144, His164	-64.6
	3	-4.56	42	Leu141, Gly143, Ser144, Cys145, Glu166	-94.6
3	2	-3.95	31	Thr25, Thr26, Thr45, Ser144	-86.8
	7	-3.87	60	Thr26, Leu141, Gly143, Ser144, Glu166	-83.3
	10	-3.61	37	Thr24, Thr26, Leu141, Asn142, Gly143	-58.7
4	1	-6.64	193	No H-bonds	-72.9
	2	-6.46	25	No H-bonds	-73.1
	4	-5.74	18	Glu166	-83.9
5	1	-3.49	85	Glu166	-25.9
	2	-3.46	94	Leu141, Gly143, Ser144	-50.5
	3	-3.38	77	Glu166, Gln189	-19.5
6	1	-3.12	62	Leu141, Gly143, His163, Glu166	-112.0
	2	-2.81	41	Asn142, Glu166	-95.0
	3	-2.76	69	Thr24, Thr26, Cys44, Thr45, Ser46	-57.4
7	1	-4.25	181	No H-bonds	-35.7
	2	-4.17	50	No H-bonds	-37.1
	3	-3.99	25	No H-bonds	-30.6
8	2	-4.39	28	Glu166, His172	-105.1
	3	-4.11	22	Glu166	-94.7
	10	-3.83	57	Thr26, Phe140, Gly143, Glu166	-66.5
9	1	-4.95	28	Thr26, Gln189	-108.2
	3	-4.78	24	His41, Asn142, His164, Glu166, Gln189	-92.3
	6	-4.02	30	Gly143, Glu166, Gln189	-136.5
10	2	-4.58	67	Asn142, His164, Glu166, Gln189	-106.1
	9	-3.85	25	Thr26, Gly143, Gln189	-77.3
	14	-3.67	24	Thr26, Gly143, His164	-75.1
11	1	-4.33	36	His164, Glu166	-97.0
	2	-4.28	40	Asn142, His164, Glu166, Gln189	-63.7
	5	-3.81	40	Thr26, Gly143, Gln189	-72.5
12	1	-5.41	37	Gly143, Glu166, Gln189, Thr190	-111.0
	2	-5.11	42	Asn142, Glu166	-119.0
	3	-4.87	29	Asn142, Gly143, Glu166, Gln189	-107.1

The created 256 poses were clustered based on their structural similarity, and each cluster was ranked in the order of BE between Mpro and each compound from *Moringa oleifera*. We selected three clusters with the largest number of poses, and the total inter fragment interaction energy (IFIE: kcal/mol) between each compound and all Mpro residues was evaluated using the FMO method. These values are listed in the last column.

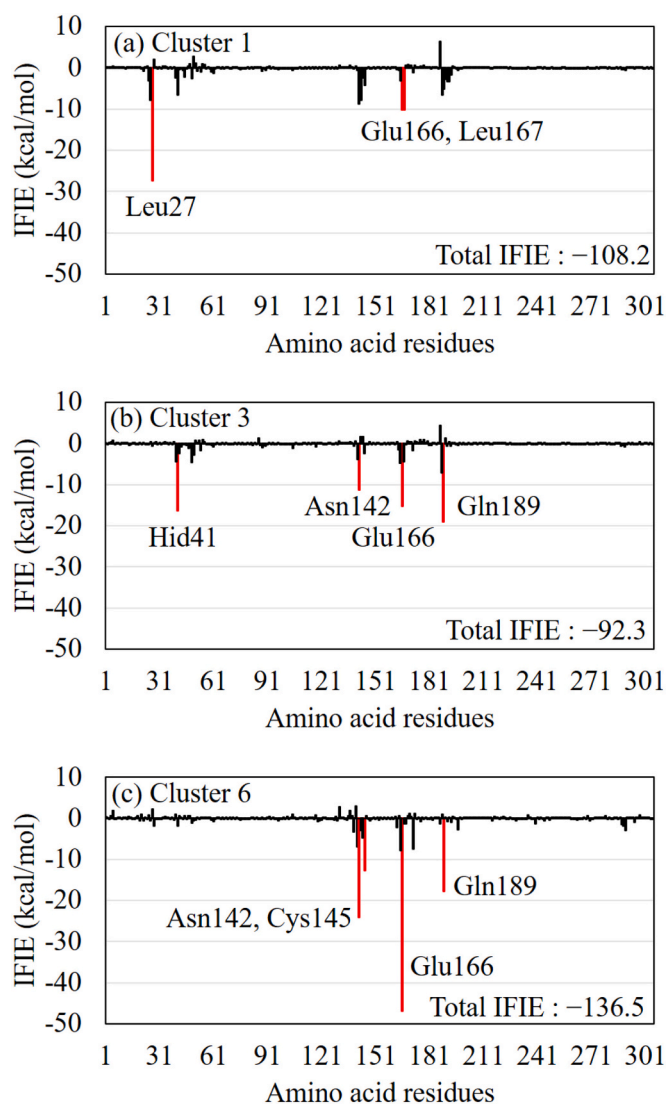


Fig. 3. The inter fragment interaction energies (IFIEs) between compound 9 and each Mpro residue for the structures of (a) cluster 1, (b) cluster 3, and (c) cluster 6. The total IFIEs between compound 9 and all Mpro residues are also shown for each cluster. The red bars indicate the residues with attractive IFIE, the size of which is larger than 10 kcal/mol. (For interpretation of the references to colour in this figure legend, the reader is referred to the web version of this article.)

2.2. *Ab initio* FMO calculations for the optimized structures of the Mpro + compound complexes

To clarify the specific interactions and binding affinity between the Mpro and the compound, we investigated the electronic properties of the Mpro + compound complexes in explicit waters using the *ab initio* FMO method [36]. This method has been applied to many biomolecules to obtain accurate results that are comparable with experimental results. Because water molecules can contribute to the specific interactions between the Mpro and the compound, the water molecules existing within 10 Å of the compound were explicitly considered. The number of water molecules used in the FMO calculations was approximately 150 for all clusters. To predict the binding affinity between the compound and the Mpro, we evaluated the total inter-fragment interaction energies (IFIEs) [37] between the compound and all the Mpro residues using the *ab initio* FMO method [36].

In this study, we did not consider the effect of entropy on the binding

affinity because a vibrational analysis for the solvated Mpro + compound complex is not practical when using the *ab initio* FMO method. Furthermore, the entropic effect is unlikely to be markedly different for each of the compounds, as they have similar chemical structures and bind to the same Mpro site. We thus investigated the total IFIEs between the Mpro residues and the compounds using *ab initio* FMO calculations and estimated the binding affinity under the assumption that the entropic effect was the same for each of the compounds.

In the FMO calculations, the MP2/6-31G(d) method [38,39] of the FMO calculation program ABINIT-MP ver.6.0 [40] was used. Each amino acid residue of the Mpro, compound, and individual water molecule were assigned to a fragment in the FMO calculations. This fragmentation enabled us to analyze the interactions between each Mpro residue and the compound affected by the solvating water molecules. In our previous study [41], the binding properties between the androgen receptor (AR) protein and its ligands were investigated using the same FMO calculations. The evaluated total IFIEs between the AR residues and the ligands were confirmed to correlate well with the binding

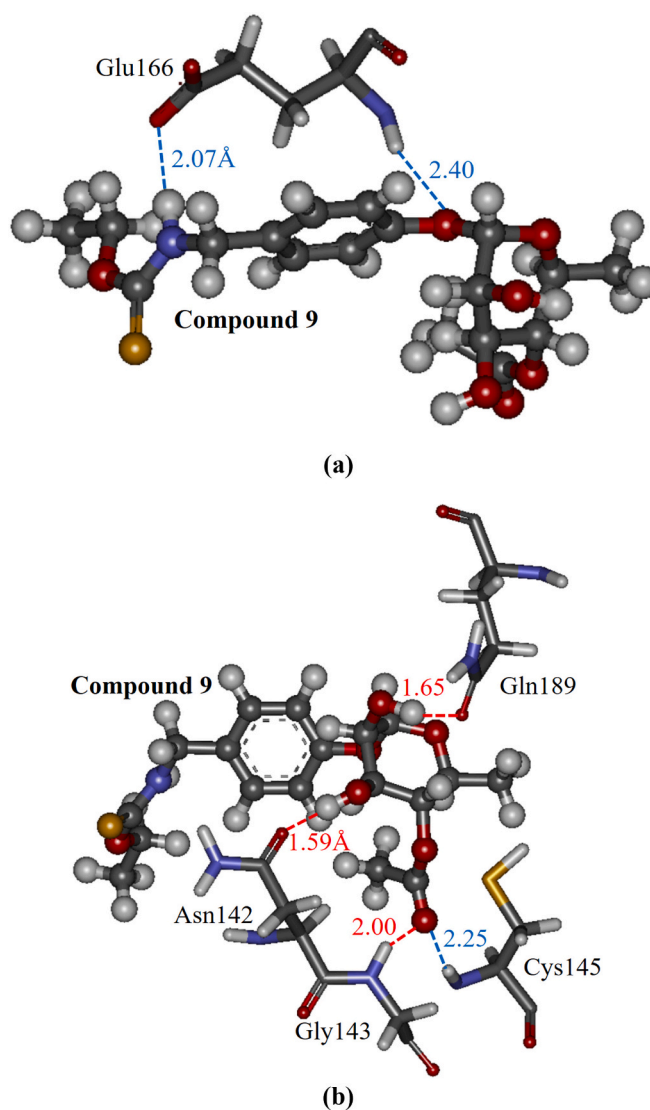


Fig. 4. The interacting structures between compound 9 (ball-and-stick model) and selected important Mpro residues (stick model) in the optimized structure of the Mpro + compound 9 complex for cluster 6. (a) Compound 9 and Glu166, and (b) compound 9 and Asn142, Gly143, Cys145, and Glu189. Hydrogen bonding and electrostatic interactions are indicated by red and blue lines, respectively. (For interpretation of the references to colour in this figure legend, the reader is referred to the web version of this article.)

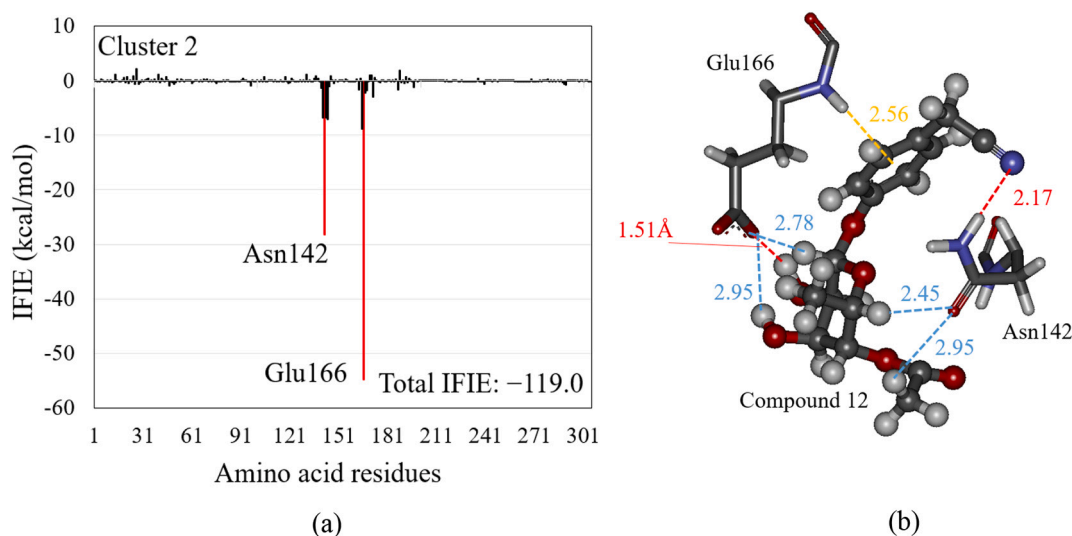


Fig. 5. (a) The inter fragment interaction energies (IFIEs) between compound 12 and each Mpro residue for the structure of cluster 2. The total IFIE between compound 12 and all Mpro residues is also shown. The red bars indicate the residues with attractive IFIE, the size of which is larger than 10 kcal/mol. (b) The interacting structures between compound 12 (ball-and-stick model) and selected important Mpro residues (stick model) in the optimized structure of the Mpro + compound 12 complex for cluster 2. Hydrogen bonding, electrostatic, and NH- π interactions are indicated by red, blue, and orange lines, respectively. (For interpretation of the references to colour in this figure legend, the reader is referred to the web version of this article.)

Table 2

The total inter fragment interaction energy (IFIE; kcal/mol) between each compound and all Mpro residues evaluated using the FMO method.

Compound	Total IFIE
9	-136.5
9a	-149.9
9b	-139.1
9c	-160.6
9d	-175.4
9e	-145.1
9f	-139.6
9g	-153.9

The proposed compounds are defined as compounds 9a–9g, based on the site to be replaced by a hydroxyl group. For example, in compound 9a, the hydrogen atom at the α -site of compound 9 shown as follows is replaced by a hydroxyl group.

affinities of these ligands obtained through experiments. The correlation coefficient (R^2) was 0.94 for all the nine different ligands, confirming that our evaluated total IFIEs can explain the trend of the observed binding affinities between AR and these ligands. Therefore, the present FMO calculations are expected to obtain accurate binding properties between Mpro residues and the compounds.

3. Results and discussion

3.1. Binding properties between Mpro and compounds contained in *Moringa oleifera*

M. oleifera is effective at inhibiting Mpro activity and contains many types of natural compounds. However, it is unclear which of these compounds is the most effective. We identified 33 compounds from the literature [18–21] and filtered them using “Lipinski’s rule of five” [22] to obtain the 12 candidate compounds for the Mpro inhibitor. Their pharmacokinetic properties evaluated using the SwissADME web tool [23] are listed in Table S1 (see SI), and their chemical structures are shown in Fig. 1. Their binding properties to the Mpro were investigated using the present *ab initio* FMO calculations to elucidate which

compound bonded the strongest to the Mpro.

Morphine (Fig. 1a) is an anti-ulcer and anti-inflammatory agent contained in *Moringa* root bark. Kaempferol (Fig. 1b) and quercetin (Fig. 1c) are flavonoids found in *Moringa* flowers [20]. The antiviral, anti-inflammatory, and anti-cancer properties of kaempferol have been reported in previous studies [42–47], whereas quercetin has been shown to reduce the replication of several respiratory viruses [48]. Pterygosperrin (Fig. 1d) is found in *Moringa* seeds and has antibacterial properties [20]. The dried leaves of *M. oleifera* are rich in polyphenols, of which phenolic acids and flavonoids are the main compounds. Gallic acid (Fig. 1f) is a phenolic acid with anti-tumor and antioxidant functions [49]. Niaziminin (Fig. 1i) is a thiocarbamate contained in *M. oleifera* leaves. Murakami et al. [50] reported that the presence of an acetoxy group at the 4'-position of niaziminin is important for the inhibition of EBV activation. It is noted that niaziminin, niazinin (Fig. 1j), and O-ethyl N-carbamothioate (Fig. 1k) possess significantly different binding properties to the Mpro, although they have similar chemical structures, as will be shown later in this study.

Using the AutoDock [31] program, each compound was docked to the ligand-binding pocket of the Mpro shown in Fig. 2. The created structures of the Mpro + compound complex were classified into several clusters according to their structural similarities, and the clusters were ranked on the basis of the lowest binding energy (BE) between the Mpro and the compound, as evaluated using AutoDock.

Table 1 lists the ranks, BEs, the number of poses, and Mpro residues involved in H-bonds with each compound for the three clusters with a larger number of poses obtained by AutoDock. In the present study, we selected these clusters because a larger number of poses indicate that the compound has a higher possibility of having one of the structures included in the cluster. In the last column of Table 1, the total IFIEs between each compound and all residues of Mpro evaluated using *ab initio* FMO method are listed. The representative structures included in the three clusters were employed as the candidate structures of the complexes in the subsequent molecular simulations.

To clarify the difference in conformation of the compound in the Mpro + compound complex for the three clusters, we compared the conformations in Fig. S1 (see SI). Small-sized compounds (compounds 5–7) were able to bind to different sites in the ligand-binding pocket of the Mpro, because the size of the pocket was larger than the size of these compounds. In contrast, as compounds 9–12 were large and had similar

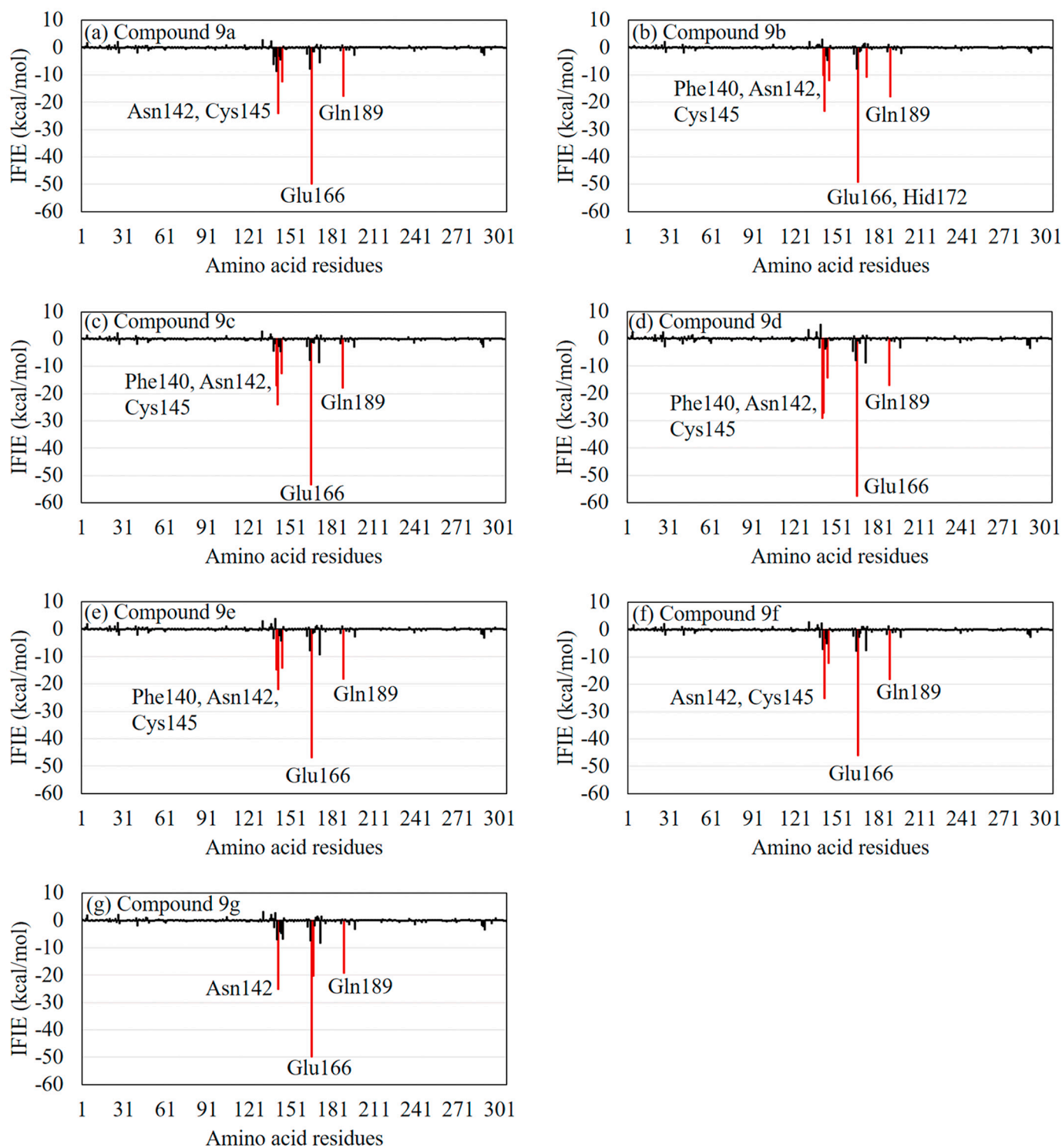


Fig. 6. The inter fragment interaction energies (IFIEs) between our proposed compound 9 derivatives and the Mpro residues. The red bars indicate the residues with attractive IFIE, the size of which is larger than 10 kcal/mol. (For interpretation of the references to colour in this figure legend, the reader is referred to the web version of this article.)

structures, they bonded to similar sites on the Mpro, although their conformations differed.

We optimized the candidate structures in explicit water molecules using the AMBER 12 [32] MM method [33–35]. For the optimized structures, the total IFIEs between the compound and all the Mpro residues were precisely evaluated using the *ab initio* FMO method [36,40] to determine which compound bonded the strongest to the Mpro. As indicated in Table 1, compound 9 had the largest total IFIEs (−136.5

kcal/mol) among the 12 compounds. The size of this value was at least 17.5 kcal/mol larger than that of the other compounds. Accordingly, it was expected that compound 9 would bond the strongest to the Mpro. Additionally, compounds 6, 8, 10, and 12 had relatively large total IFIEs.

To understand why compound 9 bonded strongly to the Mpro, we compared the conformation of compound 9 in the ligand-binding pocket of the Mpro for the three clusters obtained using AutoDock. As shown in Fig. S1(i) (see SI), in the third ranked cluster (in pink), compound 9

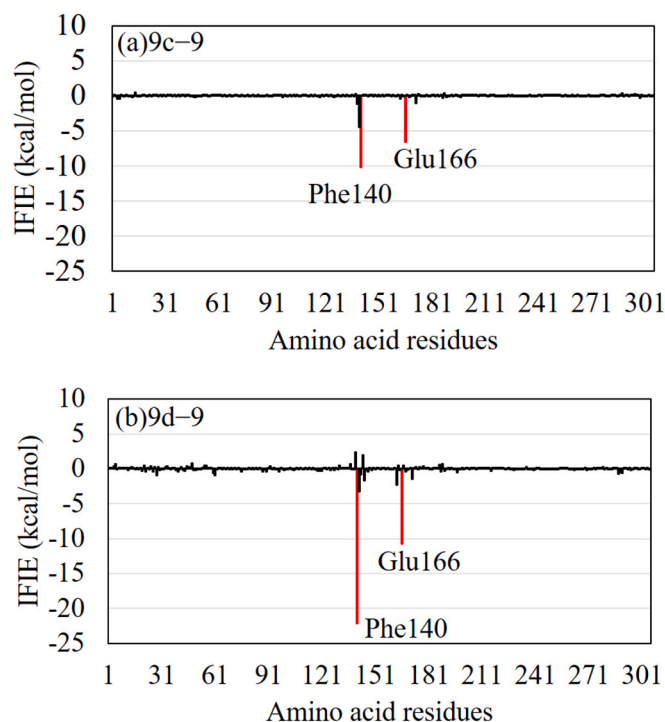


Fig. 7. The difference in inter fragment interaction energies (IFIEs) between the Mpro residues and (a) compounds 9c and 9 and (b) compounds 9d and 9. The red bars indicate the residues with IFIE difference, the size of which is larger than 5 kcal/mol. These residues interact more strongly with compound 9c/9d compared with compound 9. (For interpretation of the references to colour in this figure legend, the reader is referred to the web version of this article.)

exists near the negatively charged Glu166 residue of the Mpro and is stabilized by the electrostatic attractive interactions between it and this residue. As a result, compound 9 of the cluster 6 has the largest total IFIEs. Furthermore, we analyzed the IFIEs between the Mpro residues and compound 9 in the structures of the three clusters. As shown in Fig. 3, Asn142, Glu166, and Gln189 residues primarily contribute to the interactions with compound 9 in all the clusters. These residues were thus considered to be important for the strong binding of compound 9 to the Mpro. In the cluster 6 structure (Fig. 3c), compound 9 interacted strongly (−45 kcal/mol) with Glu166; it also interacted with Cys145. As a result, compound 9 had the largest total IFIEs in the cluster 6 structure.

Additionally, we attempted to clarify which part of compound 9 was important for its strong binding to the Mpro, to propose novel potent Mpro inhibitors based on this compound. As shown in Fig. 4a, the NH group and the oxygen atom connecting the two rings of compound 9 contribute to the strong electrostatic interactions with the backbone and the side chain of Glu166. These interactions are the main reason for compound 9 having the largest total IFIEs. Additionally, Fig. 4b reveals that Asn142, Gly143, and Gln189 of the Mpro form hydrogen bonds with the hydroxide (OH) and carbonyl groups of the cyclohexane ring of compound 9. Therefore, these groups, as well as the oxygen atom of compound 9, are considered essential for maintaining the strong binding between the compound and the Mpro residues. In contrast, as the other sites of compound 9 make no significant contribution to its binding to the Mpro, it is expected that the replacement of these sites will enhance the binding affinity of compound 9 to the Mpro.

The binding properties to the Mpro of the other compounds included in *M. oleifera* were investigated in the same manner. Their docking conformations to the Mpro, IFIEs with the Mpro residues, and their interacting structures with Mpro residues are shown in Figs. S1–S13 (see SI). As listed in the last column of Table 1, the compound 12 has the second largest total IFIE among the 12 compounds. Its IFIEs with the

Mpro residues and the interacting structure between compound 12 and some important residues are shown in Fig. 5. Compound 12 interacts strongly with Glu166 and Asn142, however, it has no significant interaction with Gln189 and Cys145 as for the compound 9. As a result, the size of total IFIE of compound 12 is remarkably smaller than that for the top ranked compound 9.

3.2. Proposal of novel potent inhibitors and their binding properties to the Mpro

As compound 9 was found to bind the strongest to the Mpro, we adopted it as a lead compound for proposing novel potent Mpro inhibitors. Fig. 4 shows that the OH groups of compound 9 contribute to its strong interactions with the Mpro residues. We thus considered the introduction of an OH group to selected sites of compound 9. The seven sites shown in Table 2 were considered because the lower part of compound 9 already contributed to the interactions with the Mpro, as shown in Fig. 4b. The proposed compounds are defined as compounds 9a – 9g, based on the site to be introduced by the OH group indicated in Table 2.

The total IFIEs between the Mpro residues and our proposed compounds, as well as compound 9, are listed in Table 2. The compounds 9d and 9c had larger total IFIEs compared with the other compounds. The size of their total IFIEs was at least 24 kcal/mol larger than that of compound 9, indicating that the introduction of an OH group enhanced the interaction between compound 9 and the Mpro residues.

To establish why compounds 9d and 9c had larger total IFIEs, we compared the IFIEs for our proposed compounds. As shown in Fig. 6, the Glu166 residue of Mpro has the strongest attractive interaction with all the compounds, indicating its importance for ligand binding of the Mpro. Specifically, compound 9d interacted strongly with Glu166. In addition, Phe140, Asn142, Cys145, and Gln189 contributed to interactions between the Mpro and compounds 9d/9c.

To elucidate the effect of the OH introduction on the IFIEs between the Mpro and compound 9, we investigated the difference in IFIEs for compounds 9, 9c, and 9d. As indicated in Fig. 7a, the effect of the OH introduction was not significant (smaller than 10 kcal/mol) for compound 9c. In contrast, Fig. 7b reveals that the interactions between compound 9 and Phe140/Glu166 of the Mpro were significantly enhanced by the introduction of OH at the d-site of compound 9.

We furthermore compared the interacting structures between these residues and compounds 9, 9c, and 9d to clarify the difference in the effect of the OH group, based on the introduced site. As shown in Fig. 8a, compound 9 interacted electrostatically with Glu166 and Phe140. Particularly, the Glu166 side chain interacted strongly with the NH group of compound 9. By introducing an OH group at the c-site of compound 9, a hydrogen bond was formed between the OH group and the oxygen atom of the Phe140 backbone (Fig. 8b). However, the interactions of the other parts of compound 9 with the Mpro residues did not change significantly due to the introduction of the OH group. In contrast, Fig. 8c elucidates that the introduction of an OH group at the d-site of compound 9 significantly enhanced the interactions between compound 9 and selected Mpro residues. The introduced OH group formed a hydrogen bond with Phe140. Additionally, the interaction between the Glu166 side chain and the NH group of compound 9 was enhanced to form a hydrogen bond at 1.78-Å distance. As a result, the IFIEs between compound 9d and Phe140/Glu166 were significantly enhanced by the OH group introduction at the d-site, leading to a larger amount of total IFIEs between the Mpro residues and compound 9d. Regarding the other proposed compounds shown in Table 2, the introduction of an OH group into compound 9 did not cause a significant change in the IFIEs and the interacting structures between compound 9 and the Mpro residues. Consequently, it is revealed that the site of the OH group replacement is important for enhancing the interactions between compound 9 and the Mpro residues, and that compound 9d binds more strongly to the Mpro than compound 9.

In order to validate the improvement of the binding affinity between

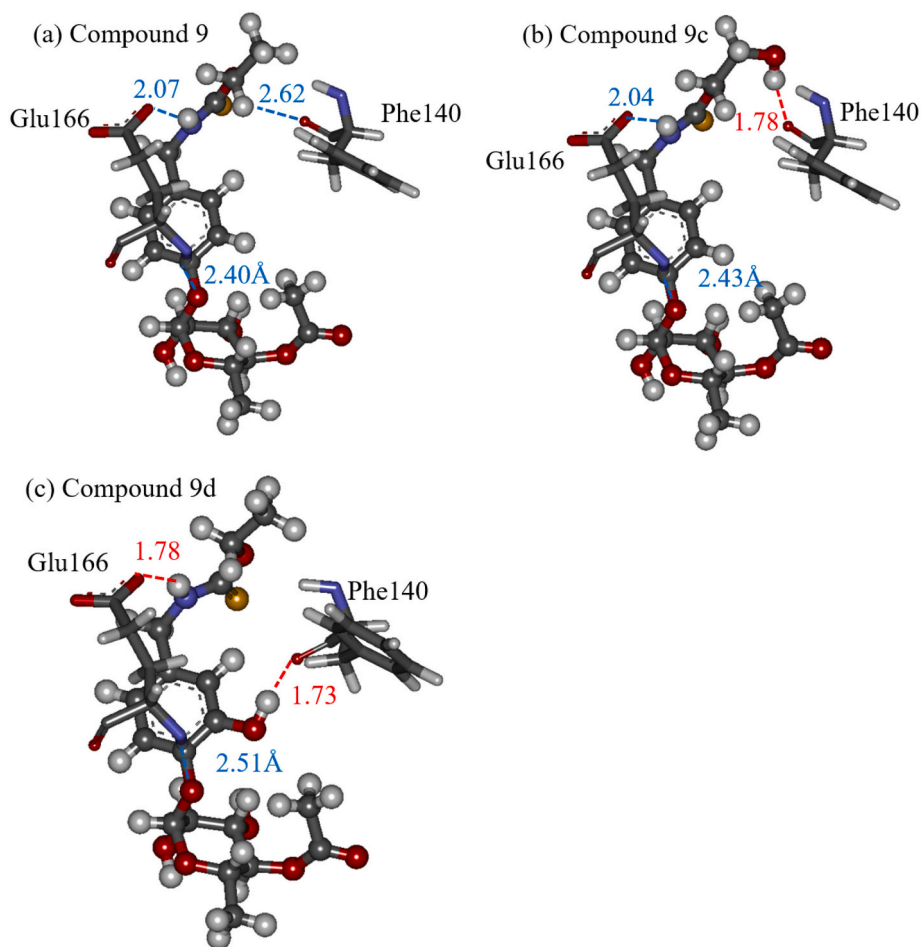


Fig. 8. The interacting structures between our proposed compounds (ball-and-stick model) and selected important Mpro residues (stick model): (a) compound 9, (b) compound 9c, and (c) compound 9d. The red and blue lines indicate hydrogen bonding and electrostatic interactions, respectively. (For interpretation of the references to colour in this figure legend, the reader is referred to the web version of this article.)

the Mpro and compound 9 by the addition of OH group, we additionally considered a methyl group and introduced it into the d-site of compound 9. The structure of its complex with the Mpro was optimized by the MM method, and the IFIEs between the Mpro and the methyl replaced compound 9 were investigated using FMO method. The total IFIE was evaluated -144.6 kcal/mol, whose size is about 30 kcal/mol smaller than that (-175.4 kcal/mol) of the OH replaced compound 9d. As shown in Fig. 8c, the OH group of compound 9d forms a hydrogen bond with the oxygen atom of Phe140 backbone. By replacing the OH group with a CH_3 group, this hydrogen bond disappears, resulting in a weaker interaction between the Mpro and the CH_3 replaced compound 9. Therefore, it is revealed that the introduction of OH group is more effective for improving the binding affinity between the Mpro and compound 9.

4. Conclusions

To propose novel natural compounds as potent inhibitors of the SARS-CoV-2 Mpro, we investigated the binding properties between the Mpro and the 12 natural compounds found in the *M. oleifera* plant, using molecular simulations based on protein–ligand docking, MM optimizations, and *ab initio* FMO calculations. The FMO results revealed that niaziminin bonded the strongest to the Mpro. Furthermore, to enhance the binding affinity of niaziminin to the Mpro, we introduced an OH group at different niaziminin sites and investigated the binding properties between these derivatives and the Mpro. Our proposed compound, which includes an OH group introduced into the phenyl ring of

niaziminin, formed hydrogen bonds with the Glu166 and Phe140 residues of the Mpro to bind more strongly to the Mpro. It is thus expected that this niaziminin derivative (compound 9d in Table 2) can be a potent inhibitor of the Mpro.

Author statement

The authors have no statement.

Declaration of Competing Interest

The authors declare that they have no known competing financial interests or personal relationships that could have appeared to influence the work reported in this paper.

Data availability

Data will be made available on request.

Appendix A. Supplementary data

Supplementary data to this article can be found online at <https://doi.org/10.1016/j.bpc.2021.106608>.

References

- [1] M. Pachetti, B. Marini, F. Benedetti, et al., Emerging SARS-CoV-2 mutation hot spots include a novel RNA-dependent-RNA polymerase variant, *J. Transl. Med.* 18 (2020) 1–9.
- [2] J. Ahmad, S. Ikram, F. Ahmad, et al., SARS-CoV-2 RNA dependent RNA polymerase (RdRp)–a drug repurposing study, *Heliyon* 6 (2020), e04502.
- [3] M. Pal, G.B. Kerors, V.A. Kandi, Knowledge update on SARS-Coronavirus-2 (SARS-CoV-2)/COVID-19 and its global public health implications, *Am. J. Clin. Med. Res.* 8 (2020) 23–27.
- [4] A. Saxena, Drug targets for COVID-19 therapeutics: ongoing global efforts, *J. Biosci.* 45 (2020) 1–24.
- [5] M. Motiwale, N.S. Yadav, S. Kumar, et al., Finding potent inhibitors for COVID-19 main protease (Mpro): an in silico approach using SARS-CoV-3CL protease inhibitors for combating CORONA, *J. Biomol. Struct. Dyn.* 7 (2020) 1–12.
- [6] W. Tachoua, M. Kabrine, M. Mushtaq, et al., An in-silico evaluation of COVID-19 main protease with clinically approved drugs, *J. Mol. Graph. Model.* 101 (2020) 107758.
- [7] R.S. Joshi, S.S. Jagdale, S.B. Bansode, et al., Discovery of potential multi-target-directed ligands by targeting host-specific SARS-CoV-2 structurally conserved main protease, *J. Mol. Graph. Model.* 5 (2020) 1–6.
- [8] K. Anand, J. Ziebuhr, P. Wadhvani, et al., Coronavirus main proteinase (3CLpro) structure: basis for design of anti-SARS drugs, *Science* 300 (2003) 1763–1767.
- [9] L. Zhang, D. Lin, X. Sun, et al., Crystal structure of SARS-CoV-2 main protease provides a basis for design of improved α -ketoamide inhibitors, *Science* 368 (2020) 409–412.
- [10] Z. Jin, X. Du, Y. Xu, et al., Structure of Mpro from COVID-19 virus and discovery of its inhibitors, *Nature* 582 (2019) 289–293.
- [11] B. Pendyala, A. Patras, In silico Screening of Food Bioactive Compounds to Predict Potential Inhibitors of COVID-19 Main protease (Mpro) and RNA-dependent RNA polymerase (RdRp), 2020, <https://doi.org/10.26434/chemrxiv.12051927.v2>.
- [12] S. Das, S. Sarmah, S. Lyndem, et al., An investigation into the identification of potential inhibitors of SARS-CoV-2 main protease using molecular docking study, *J. Biomol. Struct. Dyn.* (2020) 1–8.
- [13] M. Manish, Studies on Computational Molecular Interaction between SARS-CoV-2 Main Protease and Natural Products, 2020, <https://doi.org/10.26434/chemrxiv.12024789.v2>.
- [14] A.B. Gurung, M.A. Ali, J. Lee, et al., Unravelling lead antiviral phytochemicals for the inhibition of SARS-CoV-2 Mpro enzyme through in silico approach, *Life Sci.* 255 (2020) 117831.
- [15] Antonio A. Da Silva, L.S. Wiedemann, V.F. Veiga-Junior, Natural products' role against COVID-19, *RSC Adv.* 10 (2020) 23379–23393.
- [16] M. Vergara-Jimenez, M.M. Almatrafi, M.L. Fernandez, Bioactive components in Moringa Oleifera leaves protect against chronic disease, *Antioxidants* 6 (2017) 91.
- [17] D. Biswas, S. Nandy, A. Mukherjee, et al., Moringa oleifera lam. And derived phytochemicals as promising antiviral agents: a review, *S. Afr. J. Bot.* 129 (2020) 272–282.
- [18] C.Y. Ragasa, M.P. Medecilo, C.C. Shen, Chemical constituents of Moringa oleifera Lam. Leaves, *Der Pharma Chem.* 7 (2015) 395–399.
- [19] M. Mehra, N. Jakhar, S. Joshi, et al., Phytotherapeutic functionality of *Moringa oleifera* Lam. for health, *Int. J. Cell Sci. Mol. Biol.* 3 (2017) 1–4.
- [20] C.Y. Ragasa, V.A. Ng, C.C. Shen, Chemical constituents of Moringa oleifera lam. Seeds, *Int. J. Pharmacogn. Phytochem. Res.* 8 (2016) 495–498.
- [21] R.V. Karadi, M.B. Palkar, E.N. Gaviraj, et al., Antiuro lithiatic property of Moringa oleifera root bark, *Pharm. Biol.* 46 (2008) 861–865.
- [22] C.A. Lipinski, Drug-like properties and the causes of poor solubility and poor permeability, *J. Pharmacol. Toxicol. Methods* 44 (2000) 235–249.
- [23] A. Daina, O. Michielin, V. Zoete, SwissADME: a free web tool to evaluate pharmacokinetics, drug-likeness and medicinal chemistry friendliness of small molecules, *Sci. Rep.* 7 (2017) 42717.
- [24] D. Shaji, Computational Identification of Drug Lead Compounds for COVID-19 from *Moringa oleifera*, 2020, <https://doi.org/10.26434/chemrxiv.12535913.v1>.
- [25] S. Kim, P.A. Thiessen, E.E. Bolton, et al., PubChem substance and compound databases, *Nucleic Acids Res.* 44 (2015) D1202–D1213.
- [26] M.J. Frisch, G.W. Trucks, H.B. Schlegel, et al., Gaussian 09, Revision D. 01, Gaussian, Inc Wallingford CT, 2009.
- [27] B.H. Besler, K.M. Merz Jr., P.A. Kollman, Atomic charges derived from semiempirical methods, *J. Comput. Chem.* 11 (1990) 431–439.
- [28] Z. Jin, X. Du, Y. Xu, et al., Structure of Mpro from SARS-CoV-2 and discovery of its inhibitors, *Nature* 582 (2020) 289–293.
- [29] C.R. Søndergaard, H.M. Mats Olsson, J.H. Rostkowski, et al., Improved treatment of ligands and coupling effects in empirical calculation and rationalization of pKa values, *J. Chem. Theory Comp.* 7 (2011) 2284–2295.
- [30] H.M. Mats Olsson, C.R. Søndergaard, J.H. Rostkowski, et al., PROPKA3: consistent treatment of internal and surface residues in empirical pKa predictions, *J. Chem. Theory Comp.* 2 (2011) 525–537.
- [31] G.M. Morris, R. Huey, W. Lindstrom, et al., Autodock4 and AutoDockTools4: automated docking with selective receptor flexibility, *J. Comput. Chem.* 30 (2009) 2785–2791.
- [32] D.A. Case, T.A. Darden, T.E. Cheatham III, et al., AMBER 12 2012, University of California, San Francisco, 2010, pp. 1–826.
- [33] K. Lindorff-Larsen, S. Piana, K. Palmo, et al., Improved side-chain torsion potentials for the Amber ff99SB protein force field, *Proteins* 78 (2010) 1950–1958.
- [34] W.L. Jorgensen, J. Chandrasekhar, J.D. Madura, et al., Comparison of simple potential functions for simulating liquid water, *J. Chem. Phys.* 79 (1983) 926–935.
- [35] J. Wang, R.M. Wolf, J.W. Caldwell, P.A. Kollman, et al., Development and testing of a general Amber force field, *J. Comput. Chem.* 25 (2004) 1157–1174.
- [36] K. Kitaura, E. Ikeo, T. Asada, et al., Fragment molecular orbital method: an approximate computational method for large molecules, *Chem. Phys. Lett.* 313 (1999) 701–706.
- [37] K. Fukuzawa, Y. Komeiji, Y. Mochizuki, et al., Intra- and inter-molecular interactions between cyclic-AMP receptor protein and DNA: Ab initio fragment molecular orbital study, *J. Comput. Chem.* 27 (2006) 948–960.
- [38] Y. Mochizuki, T. Nakano, S. Koikegami, et al., A parallelized integral-direct second-order Møller-Plesset perturbation theory method with a fragment molecular orbital scheme, *Theor. Chem. Accounts* 112 (2004) 442–452.
- [39] Y. Mochizuki, S. Koikegami, T. Nakano, et al., Large scale MP2 calculations with fragment molecular orbital scheme, *Chem. Phys. Lett.* 396 (2004) 473–479.
- [40] Y. Mochizuki, K. Yamashita, T. Nakano, et al., Higher-order correlated calculations based on fragment molecular orbital scheme, *Theor. Chem. Accounts* 130 (2011) 515–530.
- [41] I. Kobayashi, R. Takeda, K. Shimamura, et al., Specific interactions between androgen receptor and its ligand: ab initio molecular orbital calculations in water, *J. Mole Graph Model.* 75 (2017) 383–389.
- [42] J. Ren, Y. Lu, Y. Qian, et al., Recent progress regarding kaempferol for the treatment of various diseases, *Exp. Ther. Med.* 18 (2019) 2759–2776.
- [43] M. Imran, A. Rauf, Z.A. Shah, et al., Chemopreventive and therapeutic effect of the dietary flavonoid kaempferol: a comprehensive review, *Phytother. Res.* 33 (2019) 263–275.
- [44] J. Li, H. Huang, M. Feng, et al., In vitro and in vivo anti-hepatitis B virus activities of a plant extract from *Geranium carolinianum* L., *Antivir. Res.* 79 (2008) 114–120.
- [45] H.J. Jeong, Y.B. Ryu, S.J. Park, et al., Neuraminidase inhibitory activities of flavonols isolated from *Rhodiola rosea* roots and their in vitro anti-influenza viral activities, *Bioorg. Med. Chem.* 17 (2009) 6816–6823.
- [46] T. Zhang, Z. Wu, J. Du, et al., Anti-Japanese-encephalitis-viral effects of kaempferol and daidzein and their RNA-binding characteristics, *PLoS One* 7 (2012), e30259.
- [47] H. Zakaryan, E. Arabyan, A. Oo, K. Zandi, Flavonoids: promising natural compounds against viral infections, *Arch. Virol.* 162 (2017) 2539–2551.
- [48] W. Wu, R. Li, X. Li, et al., Quercetin as an antiviral agent inhibits influenza A virus (IAV) entry, *Viruses* 8 (2016) 6.
- [49] Y. Zhu, Q. Yin, Y. Yang, Comprehensive investigation of *Moringa oleifera* from different regions by simultaneous determination of 11 polyphenols using UPLC-ESI-MS/MS, *Molecules* 25 (2020) 676.
- [50] A. Murakami, Y. Kitazono, S. Jiwajinda, et al., Niaziminin, a thiocarbamate from the leaves of *Moringa oleifera*, holds a strict structural requirement for inhibition of tumor-promotor-induced Epstein-Barr virus activation, *Planta Med.* 64 (1998) 319–323.